Journal of Solid State Chemistry 183 (2010) 291–303

Contents lists available at ScienceDirect

Journal of Solid State Chemistry

journal homepage: www.elsevier.com/locate/jssc

# Alkyl group dependence on structure and magnetic properties in layered cobalt coordination polymers containing substituted glutarate ligands and 4,4′-bipyridine

Joseph H. Nettleman [a], Ronald M. Supkowski [b], Robert L. LaDuca [a,*]

[a] Lyman Briggs College and Department of Chemistry, E-30 Holmes Hall, Michigan State University, East Lansing, MI 48825, USA
[b] Department of Chemistry and Physics, King's College, Wilkes-Barre, PA 18711, USA

ARTICLE INFO

*Article history:*
Received 2 July 2009
Received in revised form
9 November 2009
Accepted 13 November 2009
Available online 22 November 2009

*Keywords:*
Copper
Dicarboxylate
Bipyridine
Coordination polymer
Thermogravimetric analysis
Crystal structure
Antiferromagnetism
Ferromagnetism
Zero-field splitting

ABSTRACT

Five two-dimensional divalent cobalt coordination polymers containing 4,4′-bipyridine (bpy) and substituted or unsubstituted glutarate ligands have been prepared hydrothermally and structurally characterized by single-crystal X-ray diffraction. $[Co(mg)(bpy)]_n$ (**1**, mg=3-methylglutarate) forms a (4,4) rhomboid grid structure based on the connection of $\{Co_2(CO_2)_2\}$ dimeric units. Using the more sterically encumbered ligands 3,3-dimethylglutarate (dmg) and 3-ethyl, 3-methylglutarate (emg) generated $\{[Co(dmg)(bpy)(H_2O)]\cdot 2H_2O\}_n$ (**2**) and $\{[Co(emg)(bpy)(H_2O)]\cdot H_2O\}_n$ (**3**), respectively. These complexes manifest $\{Co(CO_2)\}_n$ chains linked into 2-D by aliphatic dicarboxylate and bpy ligands. The "tied-back" substituted glutarate ligand 1,1-cyclopentanediacetate (cda) afforded $[Co(cda)(bpy)]_n$ (**4**), and the unsubstituted glutarate (glu) generated $[Co(glu)(bpy)]_n$ (**5**), both of which exhibit a topology similar to that of **1**. The magnetic properties of complexes **1**–**4** were analyzed successfully with a recently developed phenomenological chain model accounting for both magnetic coupling ($J$) and zero-field splitting effects ($D$), even though **1** and **4** contain isolated, discrete $\{Co_2(CO_2)_2\}$ dimers. The $D$ parameter in this series varied between 21.8(8) and 48.0(9) $cm^{-1}$. However weak antiferromagnetic coupling was observed in **1** ($J$=−2.43(4) $cm^{-1}$) and **4** ($J$=−0.89(2) $cm^{-1}$), while weak ferromagnetic coupling appears to be operative in both **2** ($J$=0.324(5) $cm^{-1}$) and **3** ($J$=0.24(1) $cm^{-1}$).



## 1. Introduction

The potential utility of coordination polymers in diverse applications such as hydrogen storage [1], molecular separations [2], ion exchange [3], catalysis [4], and optical devices [5] has been a significant impetus towards the synthesis and structural characterization of these materials. Many of these phases are constructed from aromatic dicarboxylate ligands, because of their ability to provide necessary structural rigidity and the requisite charge balance [6–14]. Additionally, bridging carboxylate groups can promote magnetic superexchange between paramagnetic metal centers in this class of materials [15]. Dicarboxylate coordination polymers containing divalent cobalt atoms often show intriguing magnetic properties such as spin canting [16], metamagnetism [17], and single-chain magnetism [18]. Inclusion of neutral nitrogen-base co-ligands such as the rigid-rod tether 4,4′-bipyridine (bpy) in the coordination polymer framework can force adjustment of the carboxylate bridging mode, which can result in significant differences in magnetic properties [19].

Dual-ligand divalent coordination polymers based on aliphatic α,ω-dicarboxylates have not been as well studied as their aromatic dicarboxylate counterparts [20]. These flexible ligands can access different conformations during self-assembly, allowing the formation of coordination polymer topologies inaccessible with more rigid aromatic linkers. Increasing the steric bulk of the aliphatic α,ω-dicarboxylate ligands by alkyl group substitution can also play a major role in modifying coordination polymer topology. For instance, $[Cu_2(glutarate)_2(bpy)]_n$ [21] and $[Cu_2(2\text{-methylglutarate})_2(bpy)]_n$ [22] both display 2-D coordination polymer layers built from $\{Cu_2(CO_2)_4\}$ paddlewheel subunits linked by the aliphatic components of the dicarboxylate ligands, in turn pillared into a very rare $4^8 6^6 8$ **rob** self-penetrated topology by the bpy tethers (both originally misidentified as having $4^{12}6^3$ primitive cubic topology). In contrast, $\{[Cu(Hdmg)_2(bpy)]\cdot H_2O\}_n$ (dmg=3,3-dimethylglutarate) possesses $[Cu_2(Hdmg)_4]$ rhombs linked into a 1-D ribbon through bpy ligands, and $[Cu_2(emg)_2(bpy)]_n$ (emg=3-ethyl, 3-methylglutarate) and $[Cu_2(cda)_2(bpy)]_n$ (cda=1,1-cyclopentanediacetate) both have 2-D slab topologies built from 1-D$\{Cu_2(CO_2)_4\}$ paddlewheel ribbons linked by bpy tethers [23].

We have thus decided to probe the structural effect on divalent cobalt dual-ligand coordination polymers imparted by sterically

* Corresponding author.
*E-mail addresses:* laduca@msu.edu, laduca@chemistry.msu.edu (R.L. LaDuca).

0022-4596/$ - see front matter © 2009 Elsevier Inc. All rights reserved.
doi:10.1016/j.jssc.2009.11.015

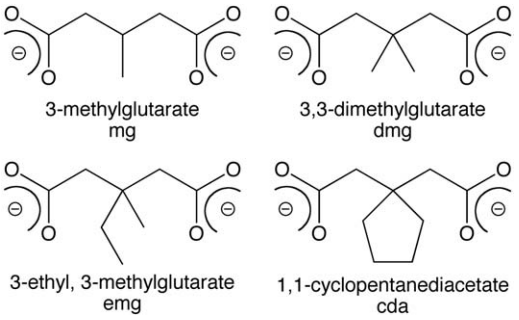


**Scheme 1.** Dicarboxylate ligands used in this study.

encumbered glutarate ligands such as 3-methylglutarate (mg), 3,3-dimethylglutarate (dmg), 3-ethyl, 3-methylglutarate (emg) and 1,1-cyclopentanediacetate (cda) (Scheme 1). In this contribution we discuss the synthesis and structural characterization of four divalent cobalt layered coordination polymers containing both substituted glutarate and rigid-rod tether 4,4′-bipyridine (bpy) ligands: $[Co(mg)(bpy)]_n$ (**1**), $\{[Co(dmg)(bpy)(H_2O)]\cdot 2H_2O\}_n$ (**2**), $\{[Co(emg)(bpy)(H_2O)]\cdot H_2O\}_n$ (**3**), and $[Co(cda)(bpy)]_n$ (**4**). Additionally, the unsubstituted glutarate (glu) derivative $[Co(glu)(bpy)]_n$ (**5**) was prepared in order to compare more fully the effect of alkyl substituents across this series of coordination polymers. The variable temperature magnetic properties of **1**–**4** are also reported and discussed.

## 2. Experimental section

### 2.1. General considerations

All chemicals were obtained from Aldrich. Water was deionized above 3 MΩ-cm in-house. Thermogravimetric analysis was performed on a TA Instruments TGA 2050 Thermogravimetric Analyzer with a heating rate of 10 °C/min up to 900 °C. Elemental analyses were carried out using a Perkin Elmer 2400 Series II CHNS/O Analyzer. IR spectra were recorded on a Perkin Elmer Spectrum One instrument on ground polycrystalline samples. Variable temperature magnetic susceptibility data (2–300 K) were collected on a Quantum Design MPMS SQUID magnetometer at an applied field of 0.1 T. After each temperature change the sample was kept at the new temperature for 5 min before magnetization measurement to ensure thermal equilibrium. The susceptibility data were corrected for filled electron shell diamagnetism using Pascal's constants [24] and for the diamagnetism of the sample holder.

### 2.2. Preparation of $[Co(mg)(bpy)]_n$ (*1*)

$Co(NO_3)_2\cdot 6H_2O$ (121 mg, 0.416 mmol), 3-methylglutaric acid (183 mg, 1.25 mmol), and 4,4′-bipyridine (195 mg, 1.25 mmol) were placed into a 10 mL of a 1:1 water:ethanol solvent mixture in a Teflon-lined 23 mL Parr acid digestion bomb. The bomb was sealed and heated at 150 °C for 24 h, whereupon it was cooled slowly in air to 25 °C. Pink crystals of **1** (130 mg, 87.0% yield based on Co) were isolated after washing with distilled water and acetone and drying in air. Anal. Calc. for $C_{16}H_{16}CoN_2O_4$ (**1**): C 53.49, H 4.49, N 7.80%, Found C 53.60, H 4.12, N 7.83%. IR ($cm^{-1}$): 3045 w, 2964 w, 1592 s, 1553 s, 1487 w, 1456 m, 1420 s, 1407 s, 1372 m, 1347 m, 1330 s, 1265 w, 1237 w, 1216 m, 1174 w, 1143 w, 1099 w, 1076 w, 1044 w, 1065 m, 1020 w, 1004 w, 936 w, 918 w, 881 w, 857 w, 845 w, 814 s, 791 m, 731 m, 713 w, 676 w, 650 m.

### 2.3. Preparation of $\{[Co(dmg)(bpy)(H_2O)]\cdot 2H_2O\}_n$ (*2*)

$Co(ClO_4)_2\cdot 6H_2O$ (152 mg, 0.415 mmol), 3,3-dimethylglutaric acid (67 mg, 0.42 mmol), and 4,4′-bipyridine (130 mg, 0.832 mmol) were placed into 10 g (555 mmol) distilled $H_2O$ in a Teflon-lined 23 mL Parr acid digestion bomb. The bomb was sealed and heated at 150 °C for 48 h, whereupon it was cooled slowly in air to 25 °C. Orange needles of **2** (54 mg, 31% yield based on Co) were isolated after washing with distilled water and acetone and drying in air. Anal. Calc. for $C_{17}H_{24}CoN_2O_7$ (**2**): C 47.78, H 5.66, N 6.56%, Found C 48.19, H 4.88, N 6.53%. IR ($cm^{-1}$): 3358 w, 2962 w, 2934 w, 1605 m, 1594 s, 1531 s, 1489 m, 1464 m, 1442 m, 1411 s, 1381 s, 1309 m, 1253 m, 1220 m, 1144 w, 1120 w, 1066 w, 1046 w, 1027 w, 1008 w, 969 w, 946 w, 916 w, 904 w, 830 s, 812 s, 769 m, 732 s, 666 s.

### 2.4. Preparation of $\{[Co(emg)(bpy)(H_2O)]\cdot H_2O\}_n$ (*3*)

$Co(NO_3)_2\cdot 6H_2O$ (136 mg, 0.467 mmol), 3-ethyl, 3-methylglutaric acid (65 mg, 0.373 mmol), and 4,4′-bipyridine (116 mg, 0.743 mmol) were placed into 10 g (555 mmol) distilled $H_2O$ in a Teflon-lined 23 mL Parr acid digestion bomb. The bomb was sealed and heated at 150 °C for 42 h, whereupon it was cooled slowly in air to 25 °C. Orange crystals of **3** (36 mg, 23% yield based on 3-ethyl, 3-methylglutaric acid) were isolated after washing with distilled water and acetone and drying in air. Anal. Calc. for $C_{18}H_{24}CoN_2O_6$ (**3**): C 51.07, H 5.72, N 6.62%, Found C 50.40, H 5.40, N 6.50%. IR ($cm^{-1}$): 3238 w, b, 2952 w, 1605 m, 1539 s, 1489 w, 1432 w, 1411 m, 1387 s, 1220 s, 1141 w, 1118 w, 1065 2, 1045 w, 1008 w, 822 m, 811 s, 756 w, 724 m, 672 m.

### 2.5. Preparation of $[Co(cda)(bpy)]_n$ (*4*)

$Co(ClO_4)_2\cdot 6H_2O$ (136 mg, 0.372 mmol), 1,1-cyclopentanediacetic acid (69 mg, 0.373 mmol), and 4,4′-bipyridine (116 mg, 0.743 mmol) were placed into 10 g (555 mmol) distilled $H_2O$ in a Teflon-lined 23 mL Parr acid digestion bomb. The bomb was sealed and heated at 150 °C for 42 h, whereupon it was cooled slowly in air to 25 °C. Orange needles of **4** (85 mg, 57% yield based on Co) were isolated after washing with distilled water and acetone and drying in air. Anal. Calc. for $C_{19}H_{20}CoN_2O_4$ (**4**): C 57.15, H 5.05, N 7.02%, Found C 53.97, H 5.11, N 6.57%. IR ($cm^{-1}$): 1604 m, 1542 s, 1486 w, 1445 m, 1414 s, 1320 w, 1222 w, 1213 w, 1172 w, 1063 m, 1007 w, 947 w, 911 w, 871 w, 811 s, 729 m, 661 m.

### 2.6. Preparation of $[Co(glu)(bpy)]_n$ (*5*)

$Co(ClO_4)_2\cdot 6H_2O$ (136 mg, 0.372 mmol), glutaric acid (49 mg, 0.37 mmol), and 4,4′-bipyridine (58 mg, 0.37 mmol) were placed into 10 g (555 mmol) distilled $H_2O$ in a Teflon-lined 23 mL Parr acid digestion bomb. The bomb was sealed and heated at 90 °C for 88 h, whereupon it was cooled slowly in air to 25 °C. Reddish pink blocks of **5** (44 mg, 36% yield based on Co) were isolated after washing with distilled water and acetone and drying in air. Anal. Calc. for $C_{15}H_{14}CoN_2O_4$ (**5**): C 52.19, H 4.09, N 8.12%, Found C 51.94, H 4.04, N 8.06%. IR ($cm^{-1}$): 3066 w, 2949 w, 2900 w, 1588 s, 1552 s, 1488 m, 1455 m, 1431 m, 1407 s, 1341 w, 1322 w, 1306 m, 1277 w, 1243 w, 1218 w, 1200 w, 1175 w, 1154 w, 1002 w, 1064 m, 1045 w, 1022 w, 1006 w, 907 m, 881 m, 857 w, 814 s, 792 m, 731 m, 658 m.

## 3. X-ray crystallography

Single crystal X-ray diffraction data for crystals of **1–5** were collected at 173 K using a Bruker-AXS Apex2 CCD instrument, using graphite-monochromated Mo$K\alpha$ radiation ($\lambda$=0.71073 Å). The data were integrated via SAINT [25]. Lorentz and polarization effect and absorption corrections were applied with SADABS [26]. The structures were solved using direct methods and refined on $F^2$

**Table 1**
Crystal and structure refinement data.

| Data | **1** | **2** |
|---|---|---|
| Empirical formula | $C_{16}H_{16}CoN_2O_4$ | $C_{17}H_{24}CoN_2O_7$ |
| Formula weight | 359.24 | 427.32 |
| Crystal morphology | pink block | orange needle |
| Crystal size (mm) | 0.30 × 0.10 × 0.10 | 0.41 × 0.10 × 0.07 |
| Crystal system | triclinic | monoclinic |
| Space group | $P\bar{1}$ | $P2/n$ |
| $a$ (Å) | 8.072(3) | 10.1354(11) |
| $b$ (Å) | 9.557(4) | 11.4156(9) |
| $c$ (Å) | 10.500(4) | 16.4322(16) |
| $\alpha$ (°) | 110.674(4) | 90 |
| $\beta$ (°) | 91.683(5) | 102.774(7) |
| $\gamma$ (°) | 103.008(5) | 90 |
| $V$ (Å$^3$) | 733.1(5) | 1854.2(3) |
| Z | 2 | 4 |
| $D_{calc}$ (g cm$^{-3}$) | 1.627 | 1.524 |
| $\mu$ (mm$^{-1}$) | 1.193 | 0.968 |
| Min./max. *trans.* | 0.914 | 0.743 |
| $h\,k\,l$ ranges | $-10 \le h \le 10$, $-12 \le k \le 12$, $-13 \le l \le 13$ | $-12 \le h \le 11$, $-11 \le k \le 13$, $-15 \le l \le 19$ |
| Total reflections | 8 255 | 10 234 |
| Unique reflections | 3 260 | 5 553 |
| $R$(int) | 0.0444 | 0.0692 |
| Parameters | 208 | 280 |
| $R_1$ (all data)[a] | 0.0729 | 0.1192 |
| $R_1$ ($I > 2\sigma(I)$)[a] | 0.0427 | 0.0587 |
| $wR_2$ (all data)[b] | 0.0965 | 0.1454 |
| $wR_2$ ($I > 2\sigma(I)$)[b] | 0.0865 | 0.1228 |
| Max./min. residual (e$^-$/Å$^3$) | 0.570/−0.387 | 0.748/−0.814 |
| G.O.F. | 1.027 | 1.056 |

| Data | **3** | **4** | **5** |
|---|---|---|---|
| Empirical formula | $C_{18}H_{24}CoN_2O_6$ | $C_{19}H_{20}CoN_2O_4$ | $C_{15}H_{14}CoN_2O_6$ |
| Formula weight | 423.32 | 399.30 | 345.21 |
| Crystal morphology | orange block | orange needle | red block |
| Crystal size (mm) | 0.43 × 0.16 × 0.11 | 0.52 × 0.12 × 0.09 | 0.41 × 0.24 × 0.17 |
| Crystal system | monoclinic | triclinic | triclinic |
| Space group | $C2/c$ | $P\bar{1}$ | $P\bar{1}$ |
| $a$ (Å) | 17.7522(4) | 8.2186(17) | 8.7387(7) |
| $b$ (Å) | 11.4275(3) | 10.987(2) | 8.7711(7) |
| $c$ (Å) | 20.0965(5) | 11.121(2) | 9.9516(8) |
| $\alpha$ (°) | 90 | 61.930(2) | 94.527(1) |
| $\beta$ (°) | 107.931(1) | 74.132(2) | 105.030(1) |
| $\gamma$ (°) | 90 | 84.151(2) | 103.127(1) |
| $V$ (Å$^3$) | 3878.82(17) | 851.8(3) | 709.68(10) |
| Z | 8 | 2 | 2 |
| $D_{calc}$ (g cm$^{-3}$) | 1.450 | 1.557 | 1.615 |
| $\mu$ (mm$^{-1}$) | 0.921 | 1.035 | 1.229 |
| Min./max. *trans.* | 0.864 | 0.674 | 0.776 |
| $h\,k\,l$ ranges | $-21 \le h \le 21$, $-13 \le k \le 13$, $-24 \le l \le 24$ | $-10 \le h \le 10$, $-12 \le k \le 14$, $0 \le l \le 14$ | $-10 \le h \le 10$, $-10 \le k \le 10$, $-11 \le l \le 11$ |
| Total reflections | 16 490 | 25 721 | 10 519 |
| Unique reflections | 3 561 | 4 020 | 2 604 |
| $R$(int) | 0.0238 | 0.0266 | 0.0192 |
| Parameters | 254 | 235 | 199 |
| $R_1$ (all data)[a] | 0.0541 | 0.0413 | 0.0202 |
| $R_1$ ($I > 2\sigma(I)$)[a] | 0.0487 | 0.0344 | 0.0195 |
| $wR_2$ (all data)[b] | 0.1498 | 0.0787 | 0.0535 |
| $wR_2$ ($I > 2\sigma(I)$)[b] | 0.1452 | 0.0750 | 0.0531 |
| Max./min. residual (e$^-$/Å$^3$) | 1.280/−0.471 | 0.384/−0.300 | 0.306/−0.176 |
| G.O.F. | 1.105 | 1.045 | 1.116 |

[a] $R_1 = \Sigma||F_o| - |F_c||/\Sigma|F_o|$.
[b] $wR_2 = \{\Sigma[w(F_o^2 - F_c^2)^2]/\Sigma[wF_o^2]^2\}^{1/2}$.

using SHELXTL [27]. All non-hydrogen atoms were refined with anisotropic thermal parameters. Hydrogen atoms bound to carbon atoms were placed in calculated positions and refined with isotropic thermal parameters using a riding model. Hydrogen atoms bound to the bound water molecules in **2** and **3** were found by Fourier difference map and subsequently restrained to fixed positions; however, hydrogen atoms for the water molecules of crystallization could not be located. Relevant crystallographic data for **1–5** are listed in Table 1.

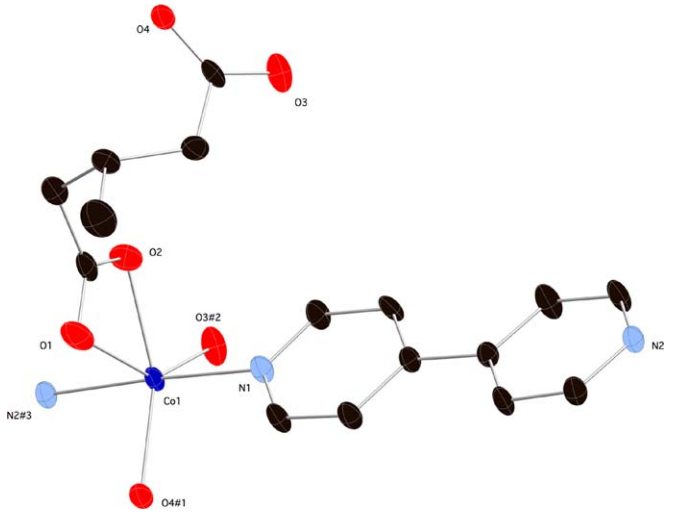


**Fig. 1.** Coordination environment of **1** with thermal ellipsoids shown at 50% probability. The symmetry codes refer to those listed in Table 2.

**Table 2**
Selected bond distance (Å) and angle (°) data for **1**.

| | | | |
|---|---|---|---|
| Co1–O4$^{\#1}$ | 2.019(2) | O3$^{\#2}$–Co1–O2 | 88.16(9) |
| Co1–O3$^{\#2}$ | 2.041(2) | O4$^{\#1}$–Co1–N2$^{\#3}$ | 85.89(9) |
| Co1–O2 | 2.076(2) | O3$^{\#2}$–Co1–N2$^{\#3}$ | 88.78(9) |
| Co1–N2$^{\#3}$ | 2.154(2) | O2–Co1–N2$^{\#3}$ | 90.13(9) |
| Co1–N1 | 2.161(2) | O4$^{\#1}$–Co1–N1 | 91.08(9) |
| Co1–O1 | 2.355(2) | O3$^{\#2}$–Co1–N1 | 93.28(9) |
| | | O2–Co1–N1 | 92.24(9) |
| O4$^{\#1}$–Co1–O3$^{\#2}$ | 121.15(9) | N2$^{\#3}$–Co1–N1 | 176.91(9) |
| O4$^{\#1}$–Co1–O2 | 150.25(9) | O4$^{\#1}$–Co1–O1 | 91.97(8) |
| N2$^{\#3}$–Co1–O1 | 90.67(9) | O3$^{\#2}$–Co1–O1 | 146.72(9) |
| N1–Co1–O1 | 88.88(9) | O2–Co1–O1 | 58.57(8) |

Symmetry equivalent positions: (#1) $x-1$, $y$, $z$; (#2) $-x+1$, $-y+2$, $-z$; (#3) $x$, $y+1$, $z+1$.

## 4. Results and discussion

### 4.1. Synthesis and spectral characterization

Hydrothermal reaction of a cobalt salt, 4,4′-bipyridine, and the requisite dicarboxylic acid generated **1–5** as crystalline solids, which were insoluble in water and common organic solvents. The infrared spectra of **1–5** (Supplementary Figs. S1–S5) were consistent with their crystal structures. Features corresponding to pyridyl ring flexing and puckering modes were observed in the region between 600 and 820 $cm^{-1}$. Medium intensity bands in the range of ~1600–1200 $cm^{-1}$ arise from stretching modes of the pyridyl rings within the bpy ligands [28]. Asymmetric and symmetric C–O stretching modes of the aliphatic dicarboxylate ligands were marked by very strong, slightly broadened bands at 1553 and 1420 $cm^{-1}$ for **1**, 1531 and 1411 $cm^{-1}$ for **2,** 1539 and 1387 $cm^{-1}$ for **3,** 1542 and 1414 $cm^{-1}$ for **4** and 1552 and 1407 $cm^{-1}$ for **5**. Broad, weak spectral features at ~3300 $cm^{-1}$ in the spectra of **2** and **3** are ascribed to the aqua ligands and unligated water molecules.

### 4.2. Structural description of $[Co(mg)(bpy)]_n$ (*1*)

The asymmetric unit of compound **1** contains one divalent cobalt atom, one fully deprotonated 3-methylglutarate (mg) ligand, and one complete bpy molecule (Fig. 1). The coordination environment at cobalt is a distorted $\{CoN_2O_4\}$ octahedron, with *trans* disposed nitrogen donor atoms from two bpy ligands. Two *cis* coordination sites are occupied by a chelating carboxylate group from one mg ligand; single oxygen donor atoms from two other mg ligands take up the remaining two *cis* positions. Bond lengths and angles about Co are consistent with octahedral coordination featuring one chelating group (Table 2).

The bis-bridging carboxylate groups of the mg ligands form $\{Co_2(CO_2)_2\}$ dimeric units, in which the Co···Co contact distance is 4.004 Å. These are linked into a 1-D $[Co(mg)]_n$ ribbon (Fig. 2) through pairs of exotridentate mg ligands via their chelating carboxylate termini. Resting in a kinked *gauche–gauche* conformation (four C-atom torsion angles=54.9°, 73.6°), the aliphatic backbones of the mg ligands provide a Co···Co interdimer closest contact distance of 6.381 Å. The ribbon motif can also be construed as being formed from the junction of eight-membered $\{Co_2(CO_2)_2\}$ and sixteen-membered $\{Co_2(OC_5O)_2\}$ cycles. Within each individual cycle rests a crystallographic inversion center, preventing chirality in **1**. The $[Co(mg)]_n$ ribbons propagate along the *a* crystal direction; the centroid-to-centroid distance between adjacent $\{Co_2(CO_2)_2\}$ dimeric units, 8.072 Å, marks the *a* lattice parameter.

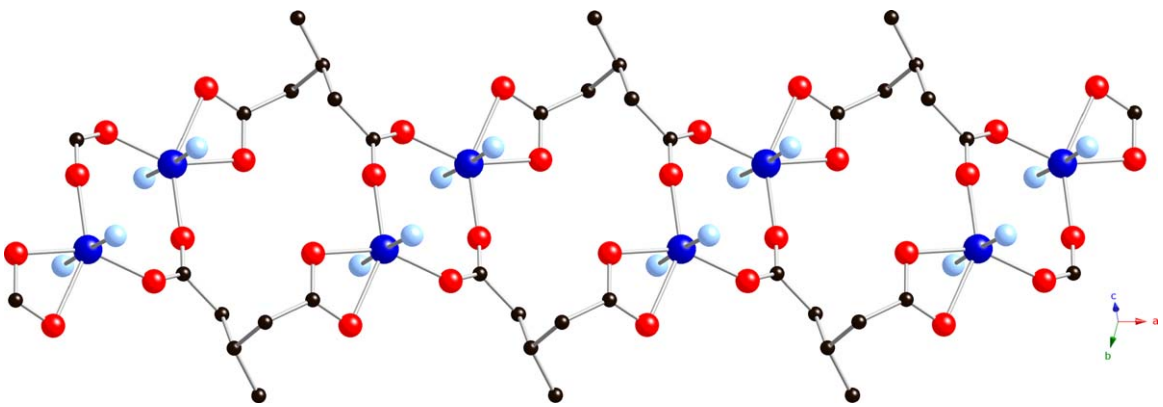


**Fig. 2.** A $[Co(mg)]_n$ ribbon motif in **1**.

In turn neighboring $[Co(mg)]_n$ ribbon motifs are conjoined into 2-D $[Co(mg)(bpy)]_n$ layers through rigid-rod bpy tethers (Fig. 3), with a through-bpy Co···Co distance of 11.434 Å. Within the 2-D layers, each $\{Co_2(CO_2)_2\}$ dimeric unit is connected to two others via mg ligands, and two others via bpy ligands. Thus the layer motif can be considered to be a (4,4) regular grid. Individual $[Co(mg)(bpy)]_n$ layers are arranged parallel to the $[01-1]$ crystal planes and stack in an *AAA* pattern along the *b* crystal direction.

The structural topology of **1** is very similar to those seen in its unsubstituted glutarate analog $[Mn(glutarate)(bpy)]_n$ [29]. The similar structure of **1** appears to indicate that the presence of a single methyl group on the glutarate backbone does not provide enough steric hindrance to alter appreciably the overarching coordination polymer topology.

### 4.3. Structural description of $\{[Co(dmg)(bpy)(H_2O)]\cdot 2H_2O\}_n$ (**2**)

The asymmetric unit of **2** contains two divalent cobalt atoms situated on crystallographic 2-fold rotation axes, two halves of two bpy ligands whose N–N axes lie along crystallographic 2-fold rotation axes, one complete dmg ligand, one aqua ligand, and two unligated water molecules, one of which is disordered over two positions in a 70/30 ratio. Operation of the crystallographic symmetry reveals octahedral $\{CoN_2O_4\}$ coordination geometries at each cobalt atom (Fig. 4). The cobalt atom Co1 is coordinated by two *trans* nitrogen donor atoms from bpy ligands, two *trans* aqua ligands, and two *trans* oxygen donor atoms from two dmg ligands. While Co2 has the same arrangement of nitrogen donor atoms, its four other coordination sites are occupied by two dmg ligands attached in a 1,5-chelating binding mode. In order to achieve this binding mode the polymethylene chain within the dmg ligand adopts a *gauche–gauche* conformation (four C-atom torsion angles=65.2°, 61.1°). Bond lengths and angles about the cobalt atoms in **2** are given in Table 3.

Extension of the structure through the 1,5-chelating/monodentate dmg ligands results in generation of a $[Co(dmg)_2Co(H_2O)_2]_n$ 1-D chain motif (Fig. 5). Embedded within the chain is a $\{Co(CO_2)\}_n$ 1-D chain pattern formed by the *anti–syn* bridging of adjacent cobalt ions by exobidentate carboxylate groups of the dmg ligands. The Co1···Co2 contact distance along the $\{Co(CO_2)\}_n$ 1-D chain is 5.134 Å; the Co···Co···Co angle along the chain measures 161.5°. The chain motifs are arranged parallel to the *a* crystal direction, with the respective Co1···Co1 or Co2···Co2 distance defining the *a* lattice parameter.

Spanning the $[Co(dmg)_2Co(H_2O)_2]_n$ 1-D ribbon patterns are sets of two crystallographically distinct bpy ligands, thereby constructing a coordination polymer slab of overall formulation $[Co(dmg)(bpy)(H_2O)_2]_n$ (Fig. 6). The inter-ring torsion angles within all of the bpy ligands are 26.8°. The Co···Co contact distances are 11.416 Å in both cases, marking the *b* lattice parameter. As each Co atom connects to four others (two through bridging carboxylates, two through bpy ligands), the overall coordination polymer topology is that of a (4,4) rhomboid grid. The grid apertures measure 11.741 × 13.248 Å, with Co···Co···Co angles around the grid perimeters of 80.8° and 99.2°.

Adjacent $[Co(dmg)(bpy)(H_2O)_2]_n$ layers stack in an *ABAB* pattern along the *c* crystal direction, related by the crystallographic 2-fold rotation axis. The water molecules of crystallization rest in the interlamellar regions, held in place by hydrogen bonding donation to the oxygen atoms of the dmg

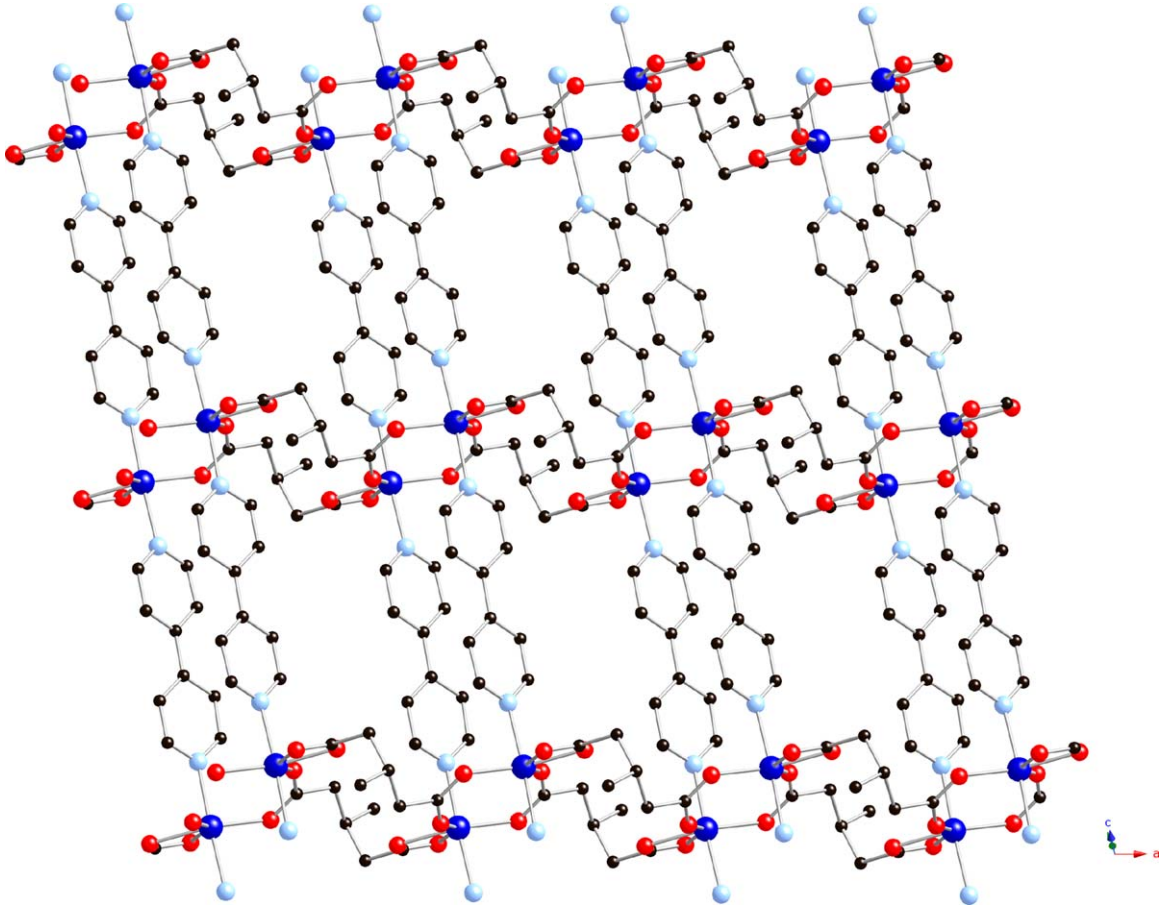


**Fig. 3.** A single $[Co(mg)(bpy)]_n$ slab motif in **1**.

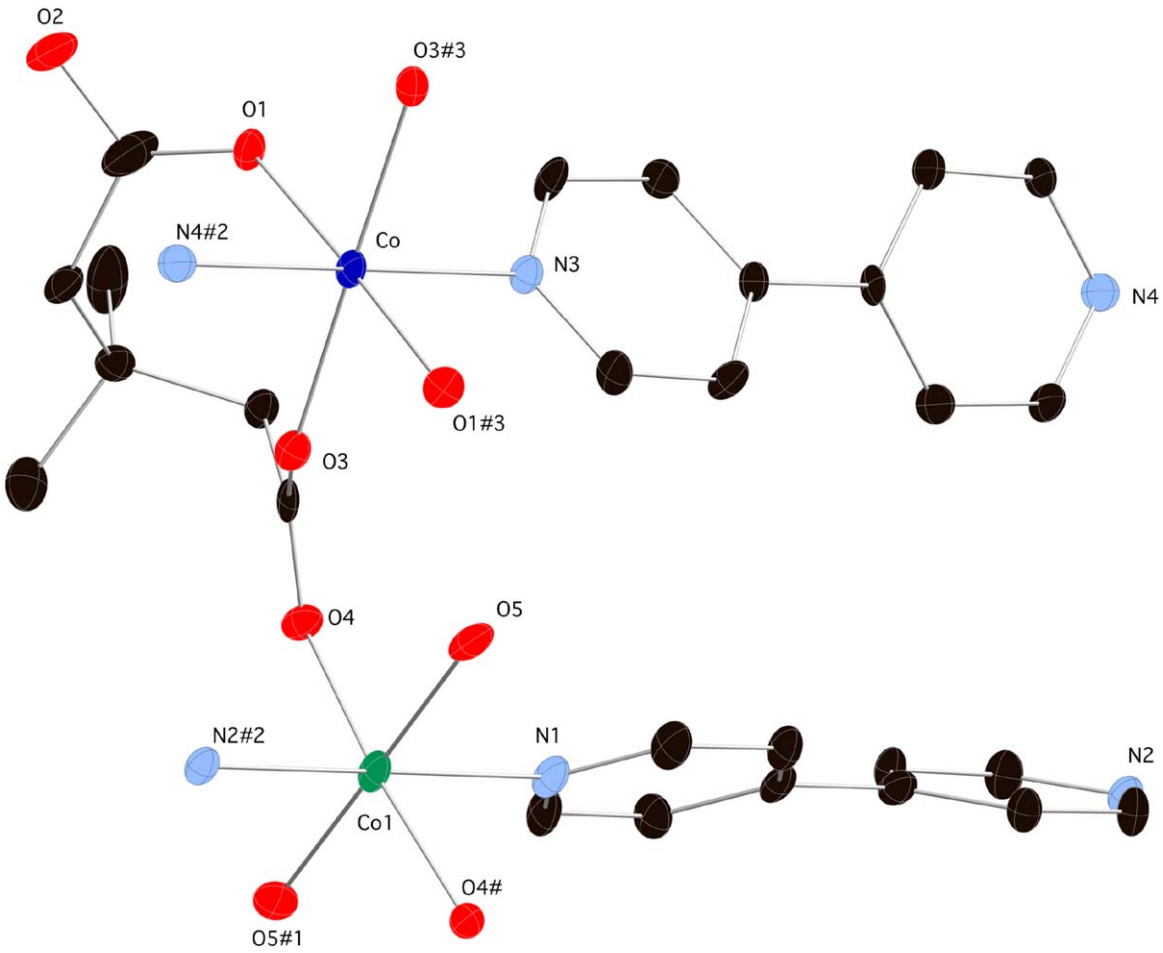


**Fig. 4.** Coordination environment of **2** with thermal ellipsoids shown at 50% probability. The symmetry codes refer to those listed in Table 3.

**Table 3**
Selected bond distance (Å) and angle (°) data for **2**.

| | | | |
|---|---|---|---|
| Co1–O5 | 2.095(4) | $O4^{\#1}$–Co1–$N2^{\#2}$ | 93.40(8) |
| Co1–$O5^{\#1}$ | 2.095(4) | O5–Co1–N1 | 90.35(8) |
| Co1–O4 | 2.106(3) | $O5^{\#1}$–Co1–N1 | 90.35(8) |
| Co1–$O4^{\#1}$ | 2.106(3) | O4–Co1–N1 | 86.60(8) |
| Co1–$N2^{\#2}$ | 2.130(5) | $O4^{\#1}$–Co1–N1 | 86.60(8) |
| Co1–N1 | 2.180(5) | $N2^{\#2}$–Co1–N1 | 180.000(1) |
| Co2–O3 | 2.072(3) | O3–Co2–$O3^{\#3}$ | 179.14(16) |
| Co2–$O3^{\#3}$ | 2.072(3) | O3–Co2–$O1^{\#3}$ | 82.97(11) |
| Co2–$O1^{\#3}$ | 2.096(3) | $O3^{\#3}$–Co2–$O1^{\#3}$ | 97.06(11) |
| Co2–O1 | 2.096(3) | O3–Co2–O1 | 97.06(11) |
| Co2–$N4^{\#2}$ | 2.151(5) | $O3^{\#3}$–Co2–O1 | 82.97(11) |
| Co2–N3 | 2.168(5) | $O1^{\#3}$–Co2–O1 | 176.93(16) |
| | | O3–Co2–$N4^{\#2}$ | 90.43(8) |
| O5–Co1–$O5^{\#1}$ | 179.31(17) | $O3^{\#3}$–Co2–$N4^{\#2}$ | 90.43(8) |
| O5–Co1–O4 | 83.83(12) | $O1^{\#3}$–Co2–$N4^{\#2}$ | 88.46(8) |
| $O5^{\#1}$–Co1–O4 | 96.21(12) | O1–Co2–$N4^{\#2}$ | 88.46(8) |
| O5–Co1–$O4^{\#1}$ | 96.21(12) | O3–Co2–N3 | 89.57(8) |
| $O5^{\#1}$–Co1–$O4^{\#1}$ | 83.83(12) | $O3^{\#3}$–Co2–N3 | 89.57(8) |
| O4–Co1–$O4^{\#1}$ | 173.20(15) | $O1^{\#3}$–Co2–N3 | 91.54(8) |
| O5–Co1–$N2^{\#2}$ | 89.65(8) | O1–Co2–N3 | 91.54(8) |
| $O5^{\#1}$–Co1–$N2^{\#2}$ | 89.65(8) | $N4^{\#2}$–Co2–N3 | 180.000(1) |
| O4–Co1–$N2^{\#2}$ | 93.40(8) | | |

Symmetry equivalent positions: (#1) $-x+3/2, y, -z+1/2$; (#2) $x, y-1, z$; (#3) $-x+5/2, y, -z+1/2$.

ligands and hydrogen bonding acceptance from the aqua ligands on Co1. According to a calculation performed using PLATON [30], the unligated water molecules occupy 10.2% of the unit cell volume.

It is apparent that the enhanced steric hindrance imparted by the dmg ligands in **2**, as opposed to the mg ligands in **1**, provokes a substantial alteration in coordination polymer structure. It is plausible that the presence of two *gem*-disposed methyl groups prevents the formation of the $\{Co_2(CO_2)_2\}$ dimeric units seen in **1**, resulting in $\{Co(CO_2)\}_n$ 1-D chain patterns instead.

### 4.4. Structural description of $\{[Co(emg)(bpy)(H_2O)]\cdot H_2O\}_n$ (**3**)

The asymmetric unit of **3** contains one divalent cobalt atom (Co1) situated on a crystallographic 2-fold rotation axis, a second divalent cobalt atom (Co2) sited on a crystallographic inversion center, one complete emg ligand, one-half of a bpy ligand situated across the 2-fold axis, one-half of a bpy ligand positioned across the inversion center, one aqua ligand (on Co2), and one water molecule of crystallization. The symmetry operations generate octahedral $\{CoN_2O_4\}$ coordination geometries at each cobalt atom (Fig. 7). Co1 is bound by four carboxylate oxygen atoms belonging to two emg ligands in a 1,5-chelating binding mode, and two bpy nitrogen donors oriented in a *trans* fashion. Similar to **2**, the polymethylene chain within the aliphatic dicarboxylate ligand rests in a *gauche–gauche* conformation (four C-atom torsion angles=64.6°, 61.9°). In contrast, Co2 is coordinated by two *trans* nitrogen donor atoms from bpy ligands, two *trans* aqua ligands, and two *trans* carboxylate oxygen atoms from two emg ligands. Pertinent bond lengths and angles about the cobalt atoms in **3** are given in Table 4.

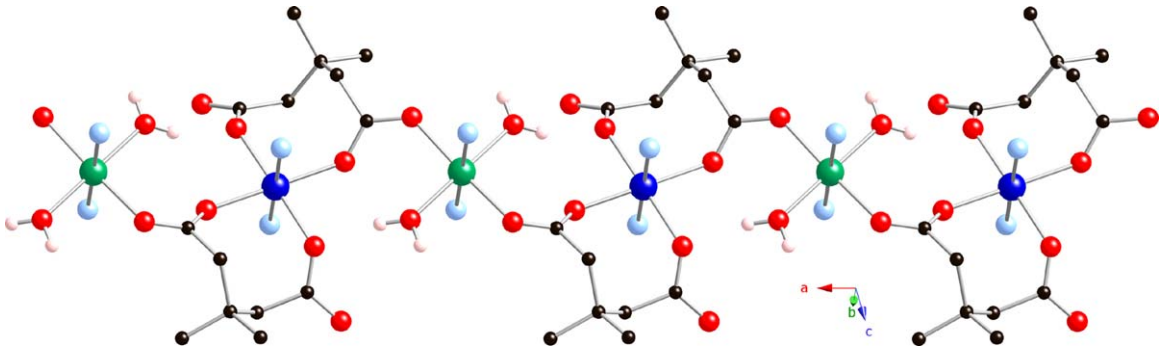

**Fig. 5.** A single $\{[Co(dmg)_2][Co(H_2O)_2]\}_n$ neutral chain motif in **2**.

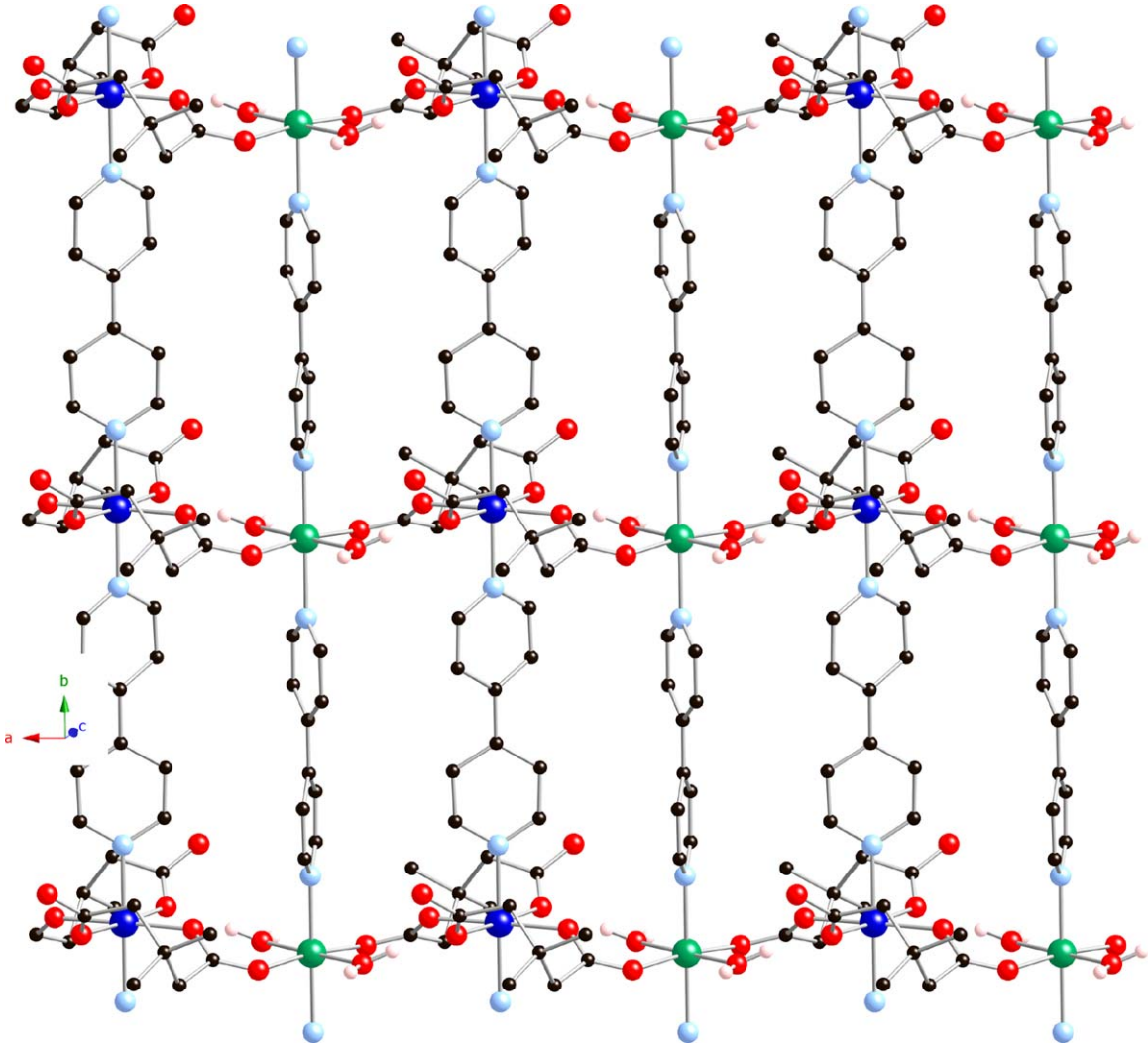

**Fig. 6.** View down *c* of the 2-D $[Co(dmg)(H_2O)(bpy)]_n$ coordination polymer layer in **2**.

As in **2**, the dicarboxylate ligands adopt an exotridentate 1,5-chelating/monodentate binding mode. $[Co(emg)_2Co(H_2O)_2]_n$ 1-D chain motifs (Fig. 8) are therefore constructed; these are oriented along the *c* crystal direction. Adjacent Co atoms are linked by emg carboxylate termini through an *anti–syn* bridging mode, resulting in a $\{Co(CO_2)\}_n$ 1-D chain pattern. The Co1···Co2 contact distance along the chain motif is 5.144 Å. The Co1···Co2···Co1 angles along the chain are perfectly linear by crystallographic symmetry, however, the Co2···Co1···Co2 angles are 155.2°. The next-nearest neighbor Co1···Co1 or Co2···Co2 distance defines the *c* lattice parameter, which is approximately twice as long as the comparable *a* lattice parameter in **2**. Although the chain pattern in **3** is structurally similar to that in **2**, deviations in the Co···Co···Co angles fostered by the greater steric bulk of the substituents on the aliphatic dicarboxylate chain result in an increase in crystallographic symmetry in **3**.

Abutting $[Co(emg)_2Co(H_2O)_2]_n$ 1-D chains are pillared by bpy ligands, resulting in a 2-D (4,4) rhomboid grid coordination polymer with stoichiometry $[Co(emg)(bpy)(H_2O)_2]_n$ (Fig. S6), very

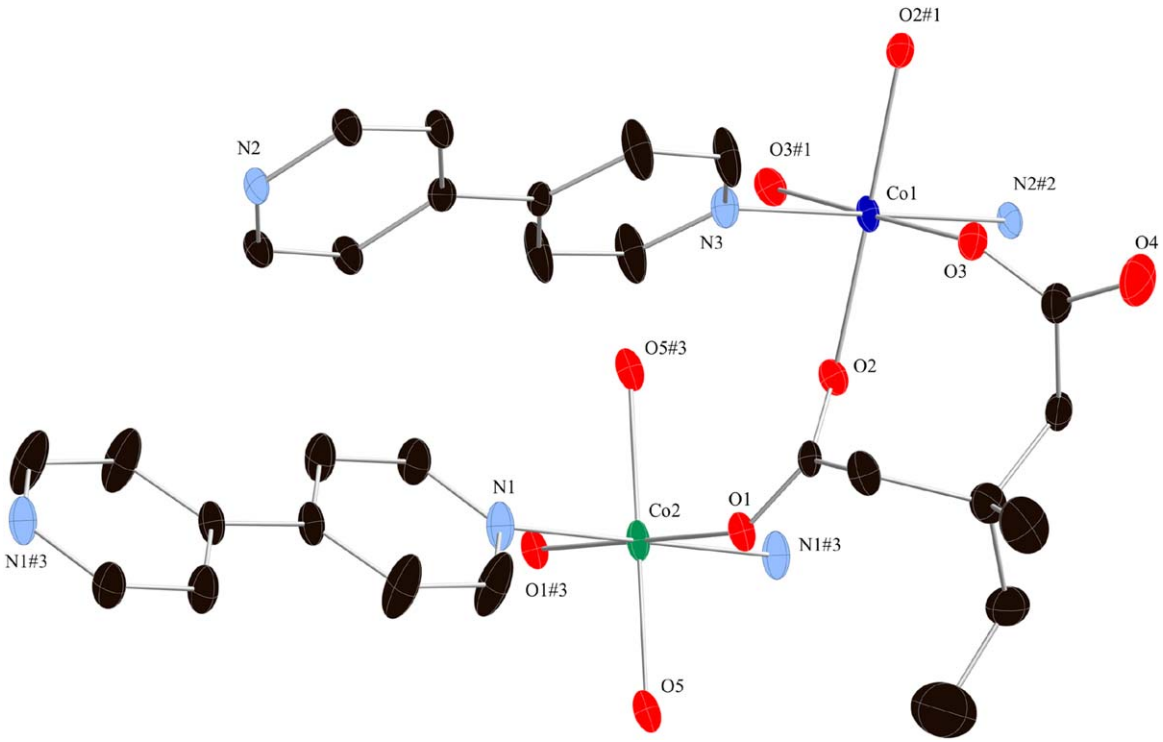


**Fig. 7.** Coordination environment of **3** with thermal ellipsoids shown at 50% probability. The symmetry codes refer to those listed in Table 4.

**Table 4**
Selected bond distance (Å) and angle (°) data for **3**.

| | | | |
|---|---|---|---|
| Co1–O2$^{\#1}$ | 2.077(2) | O3$^{\#1}$–Co1–N2 | 88.49(6) |
| Co1–O2 | 2.078(2) | O2$^{\#1}$–Co1–N3$^{\#2}$ | 89.49(6) |
| Co1–O3 | 2.105(2) | O2–Co1–N3$^{\#2}$ | 89.50(6) |
| Co1–O3$^{\#1}$ | 2.105(2) | O3–Co1–N3$^{\#2}$ | 91.51(6) |
| Co1–N2 | 2.148(3) | O3$^{\#1}$–Co1–N3$^{\#2}$ | 91.51(6) |
| Co1–N3$^{\#2}$ | 2.168(4) | N2–Co1–N3$^{\#2}$ | 180.000(1) |
| Co2–O1 | 2.062(2) | O1–Co2–O1$^{\#3}$ | 180.0 |
| Co2–O1$^{\#3}$ | 2.062(2) | O1–Co2–O5$^{\#3}$ | 82.52(9) |
| Co2–O5$^{\#3}$ | 2.121(3) | O1$^{\#3}$–Co2–O5$^{\#3}$ | 97.48(9) |
| Co2–O5 | 2.121(3) | O1–Co2–O5 | 97.48(9) |
| Co2–N1 | 2.162(3) | O1$^{\#3}$–Co2–O5 | 82.52(9) |
| Co2–N1$^{\#3}$ | 2.162(3) | O5$^{\#3}$–Co2–O5 | 180.0 |
| | | O1–Co2–N1 | 88.92(9) |
| O2$^{\#1}$–Co1–O2 | 178.99(12) | O1$^{\#3}$–Co2–N1 | 91.07(9) |
| O2$^{\#1}$–Co1–O3 | 82.76(9) | O5$^{\#3}$–Co2–N1 | 90.04(11) |
| O2–Co1–O3 | 97.27(9) | O5–Co2–N1 | 89.96(11) |
| O2$^{\#1}$–Co1–O3$^{\#1}$ | 97.27(9) | O1–Co2–N1$^{\#3}$ | 91.08(9) |
| O2–Co1–O3$^{\#1}$ | 82.76(9) | O1$^{\#3}$–Co2–N1$^{\#3}$ | 88.92(9) |
| O3–Co1–O3$^{\#1}$ | 176.98(12) | O5$^{\#3}$–Co2–N1$^{\#3}$ | 89.96(11) |
| O2$^{\#1}$–Co1–N2 | 90.51(6) | O5–Co2–N1$^{\#3}$ | 90.04(11) |
| O2–Co1–N2 | 90.50(6) | N1–Co2–N1$^{\#3}$ | 180.0 |
| O3–Co1–N2 | 88.49(6) | | |

Symmetry equivalent positions: (#1) $-x$, $y$, $-z+1/2$; (#2) $x$, $y+1$, $z$; (#3) $-x$, $-y+2$, $-z$.

similar to that seen in **2**. Thus, the slightly greater steric bulk of the ethyl group does not appear to dramatically affect the underlying coordination polymer structure. The grid apertures in **3** measure 11.482 × 13.501 Å, with Co···Co···Co angles around the grid perimeters of 77.6° and 102.4° indicating a more pinched rhomboid grid than evident in **2**. The inter-ring torsion angles within the bpy ligands are substantially narrower than in **2** (2.7°, 8.0°). The Co···Co contact distances are 11.427 Å in both cases, marking the *b* lattice parameter. The individual [Co(emg)(bpy)($H_2O$)$_2$]$_n$ layers stack in an *ABAB* pattern along the *a* crystal direction, with isolated water molecules of crystallization situated in the interlayer regions and anchored to the coordination polymer layers by hydrogen bonding. The unligated water molecules in **3** occupy 5.5% of the unit cell volume, a value approximately half of that in **2**. It is likely that the additional steric encumbrance imparted by the ethyl groups of the emg ligands does reduce the solvent accessible interlayer space, although the molecular connectivity of **3** is similar to that of **2**.

### 4.5. Structural description of [Co(cda)(bpy)]$_n$ (**4**)

Compound **4** crystallizes in the centrosymmetric triclinic space group with an asymmetric unit containing one divalent cobalt atom, one 1,1-cyclopentanediacetate (cda) ligand, and one ligated bpy moiety (Fig. 9). The coordination environment is best described as a distorted {$CoN_2O_4$} octahedron, with two bpy ligands providing the two *trans* disposed nitrogen donors. Two of the four remaining coordination sites are occupied by a chelating carboxylate group from one cda ligand. Oxygen donor atoms from two other cda ligands take up the remaining two positions. Bond lengths and angles about Co are consistent with octahedral coordination featuring one chelating group (Table 5).

Bis-bridging carboxylate groups of pairs of cda ligands link neighboring Co atoms in a *syn–syn* orientation to construct {$Co_2(CO_2)_2$} dimeric kernels with a Co···Co contact distance of 4.243 Å. Although these dimers are similar to those seen in **1**, the Co···Co distance in **4** is over 0.2 Å longer. Through the chelating carboxylate groups of the cda ligands, neighboring dimers are linked into a 1-D [Co(cda)]$_n$ ribbon (Fig. 10). The aliphatic chain of the cda ligands rests in a twisted *gauche–gauche* conformation (four C-atom torsion angles=64.3°, 68.7°), giving a Co···Co interdimer closest contact distance of 6.548 Å.

Adjacent [Co(cda)]$_n$ ribbons are pillared into 2-D [Co(cda)(bpy)]$_n$ coordination polymer slabs (Fig. S7) through the bpy tethers; the through-bpy Co···Co distance of 11.375 Å. The slab pattern of **4** is very similar to that seen in the single methyl group

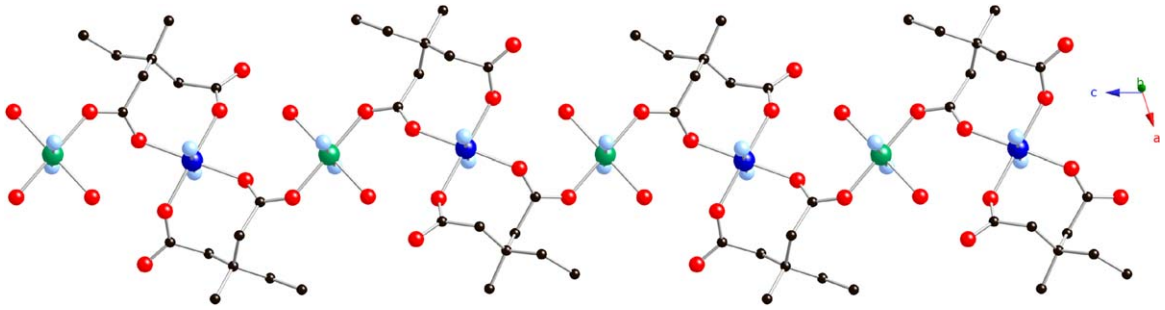

**Fig. 8.** A single $\{[Co(emg)_2][Co(H_2O)_2]\}_n$ neutral chain motif in **3**.

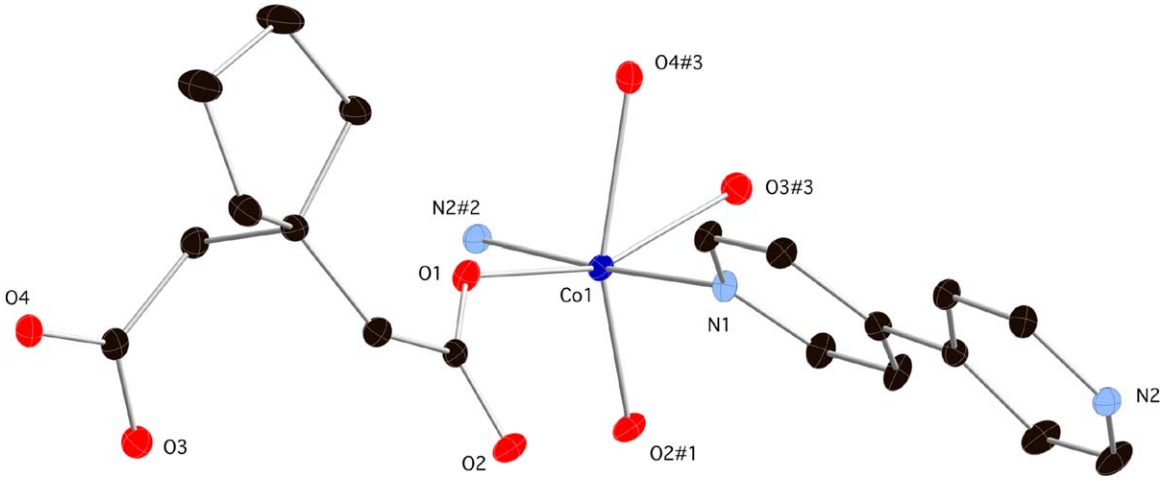


**Fig. 9.** Coordination environment of **4** with thermal ellipsoids shown at 50% probability. The symmetry codes refer to those listed in Table 5.

**Table 5**
Selected bond distance (Å) and angle (°) data for **4**.

| | | | |
|---|---|---|---|
| Co1–O2$^{\#1}$ | 2.0150(15) | O1–Co2–N1 | 91.16 |
| Co1–O1 | 2.0445(15) | N2$^{\#2}$–Co2–N1 | 176.77(7) |
| Co1–N2$^{\#2}$ | 2.1299(16) | O2$^{\#1}$–Co2–O3$^{\#3}$ | 93.84(6) |
| Co1–N1 | 2.1435(17) | O1–Co2–O3$^{\#3}$ | 157.24(6) |
| Co1–O3$^{\#3}$ | 2.1514(16) | N2$^{\#2}$–Co2–O3$^{\#3}$ | 91.69(6) |
| Co1–O4$^{\#3}$ | 2.2203(15) | N1–Co2–O3$^{\#3}$ | 87.29(6) |
| | | O2$^{\#1}$–Co2–O4$^{\#3}$ | 153.73(6) |
| O2$^{\#1}$–Co2–O1 | 108.92(6) | O1–Co2–O4$^{\#3}$ | 97.19(6) |
| O2$^{\#1}$–Co2–N2$^{\#2}$ | 88.88(6) | N2$^{\#2}$–Co2–O4$^{\#3}$ | 88.96(6) |
| O1–Co2–N2$^{\#2}$ | 88.59(6) | N1–Co2–O4$^{\#3}$ | 87.88(6) |
| O2$^{\#1}$–Co2–N1 | 94.25(6) | O3–Co2–O4$^{\#3}$ | 60.07(5) |

Symmetry equivalent positions: (#1) $-x+2$, $-y+1$, $-z$; (#2) $x$, $y+1$, $z-1$; (#3) $x+1$, $y$, $z$.

substituted derivative **1**, despite the presence of the cyclopentane ring. Apparently, "tying back" the alkyl substituents within a cyclopentane ring reduces the overall steric bulk, preventing the $\{Co(CO_2)\}_n$ 1-D chain sub-structures seen in both **2** and **3**. Within the 2-D layers, each $\{Co_2(CO_2)_2\}$ dimeric unit is connected to two others via cda ligands, and two others via bpy ligands. Thus the layer motif can be considered to be a (4,4) regular grid. Individual $[Co(cda)(bpy)]_n$ layers are arranged parallel to the $[01\bar{1}]$ crystal planes and stack in an *AAA* pattern along the *b* crystal direction.

### 4.6. Structural description of $[Co(glu)(bpy)]_n$ (**5**)

As the unsubsituted glutarate congener in this series has not yet been reported, its synthesis was attempted. Single-crystal X-ray diffraction revealed that the gross topology of **5** is a dimer-based layered structure similar to its manganese analog [29] and also to that of the methyl-substituted compound **1**. Bond lengths and angles are given in Table 6; a representation of the $\{CoO_4N_2\}$ coordination environments and dimer subunit is depicted in Fig. 11. The Co···Co through-space distance across the $\{Co(OCO)\}_2$ dimer units is 4.050 Å, only 0.046 Å longer than in **1**. In marked contrast to both **1** and $[Mn(glu)(bpy)]_n$, in which the aliphatic chains lie in a *gauche–gauche* conformation, the exotridentate chelating/bis(bridging) glutarate ligands in **5** adopt a *gauche–anti* conformation (torsion angles=71.6°, 165.8°). This more splayed-open glutarate conformation results in an inter-dimer separation of 8.771 Å along the $[Co(glu)]_n$ 1-D chain units (Fig. 12), ~0.7 Å longer than the comparable distance in **1**. These $[Co(glu)]_n$ chains are further connected into the 2-D coordination polymer structure of **5** by pillaring bpy ligands (Fig. S8).

### 4.7. Magnetic properties

Variable temperature magnetic studies were undertaken to probe the extent of spin communication within the $\{Co_2(OCO)_2\}$ dimers in **1** and **4**, and along the $\{Co(OCO)\}_n$ chains in **2** and **3**. The variable temperature magnetic susceptibility data of compound **1** followed the Curie–Weiss law for $T \geq 5$ K, with $C=2.58\ cm^3\ K\ mol^{-1}$ and $\Theta=-5.4$ K (Fig. S3), indicating antiferromagnetic coupling within the $\{Co_2(OCO)_2\}$ dimers and/or single-ion zero-field splitting effects (Fig. S9). The $\chi_m T(T)$ data for **1** show a value of $2.77\ cm^3\ K\ mol^{-1}$ at 300 K, which slowly decreases to $2.50\ cm^3\ K\ mol^{-1}$ at 60 K, and more rapidly decreases to $0.32\ cm^3\ K\ mol^{-1}$ at 2 K. This behavior is ascribed to antiferromagnetic coupling

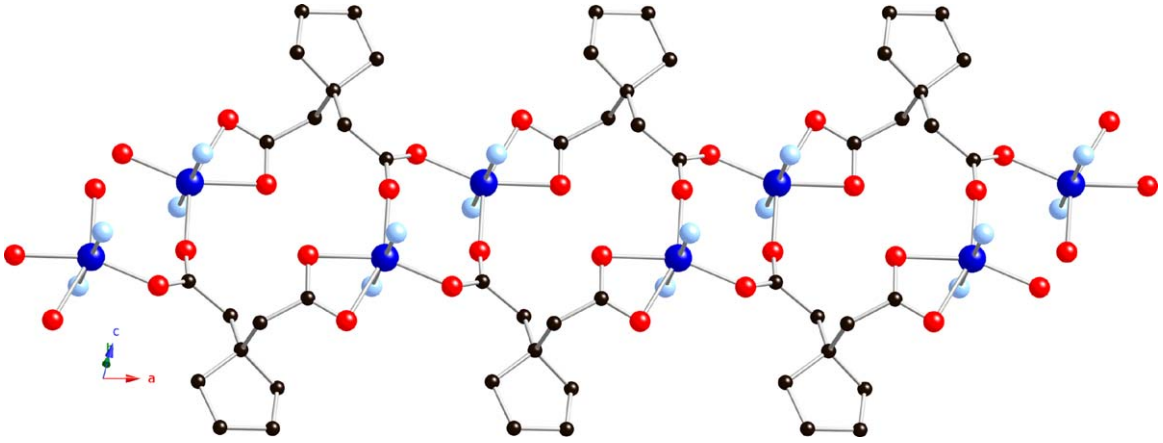


**Fig. 10.** A single $[Co(cda)(bpy)]_n$ chain motif in **4**.

**Table 6**
Selected bond distance (Å) and angle (°) data for **5**.

| | | | |
|---|---|---|---|
| Co1–O1 | 2.0201(10) | $O2^{\#1}$–Co1–$N2^{\#2}$ | 94.41 |
| Co1–$O2^{\#1}$ | 2.0474(10) | N1–Co1–$N2^{\#2}$ | 177.01(4) |
| Co1–N1 | 2.1442(12) | O1–Co1–$O4^{\#3}$ | 91.63(4) |
| Co1–$N2^{\#2}$ | 2.1529(12) | $O2^{\#1}$–Co1–$O4^{\#3}$ | 148.82(4) |
| Co1–$O4^{\#3}$ | 2.1891(10) | N1–Co1–$O4^{\#3}$ | 90.27(4) |
| Co1–$O3^{\#3}$ | 2.1892(11) | $N2^{\#2}$–Co1–$O4^{\#3}$ | 89.58(4) |
| | | O1–Co1–$O3^{\#3}$ | 151.32(4) |
| O1–Co1–$O2^{\#1}$ | 119.24(4) | $O2^{\#1}$–Co1–$O3^{\#3}$ | 89.43(4) |
| O1–Co1–N1 | 87.13(4) | N1–Co1–$O3^{\#3}$ | 95.16(4) |
| $O2^{\#1}$–Co1–N1 | 87.26(4) | $N2^{\#2}$–Co1–$O3^{\#3}$ | 87.34(4) |
| O1–Co1–$N2^{\#2}$ | 89.89(4) | $O4^{\#3}$–Co1–$O3^{\#3}$ | 59.83(4) |

Symmetry equivalent positions: (#1) $-x$, $-y+1$, $-z$; (#2) $x-1$, $y$, $z-1$; (#3) $-x$, $-y+2$, $-z$.

between $S=3/2$ divalent cobalt atoms, in tandem with the splitting of this state into an $S=1/2$ Kramers doublet at lower temperatures ($D$ parameter) [24].

An attempt was made to fit the $\chi_m T(T)$ data for **1** to an equation for an isotropic Heisenberg dimer of $S=3/2$ spins (Eq. (1)), resulting in $g=2.397(5)$ and $J=-2.51(4)\,cm^{-1}$ but with an unacceptably high $R$ value of 0.012 ($R=\{\Sigma[(\chi_m T)_{obs}-(\chi_m T)_{calc}]^2/\Sigma[(\chi_m T)_{obs}]^2\}^{1/2}$). It is clear that single-ion effects cannot be neglected in this system, due to significant deviations from ideal octahedral coordination geometry.

$$\chi_m T = \frac{Ng^2\beta^2}{k}\left(\frac{e^x+5e^{3x}+14e^{6x}}{1+3e^x+5e^{3x}+7e^{6x}}\right) \quad (1)$$

where $x=J/kT$.

As a result of the poor fit, another magnetic model was sought that could accommodate both magnetic superexchange and zero-field splitting. The phenomenological Rueff model (Eq. (2)) has been primarily used to model the magnetic behavior of 1-D divalent cobalt chains [31]. Nevertheless it was highly effective for modeling the magnetic susceptibility of dimer-based **1** over the entire temperature regime (Fig. 13), giving $D=21.8(8)\,cm^{-1}$, $J=-2.43(4)\,cm^{-1}$, and $C=2.91(2)\,cm^3\,K\,mol^{-1}$ (which gives $g=2.49(2)$), with a substantially improved $R$ value ($5.87\times10^{-4}$).

$$\chi_m T = A\exp(-D/kT)+B\exp(J/kT) \quad (2)$$

where $A+B=C=(5Ng^2\beta^2/4k)$.

The variable temperature magnetic susceptibility data (for $T\geq10\,K$) of compound **2** were also fit acceptably to the Curie–Weiss law (Fig. S10), affording $C=2.76\,cm^3\,K\,mol^{-1}$ and $\Theta=-10.9\,K$, a preliminary indication of possible antiferromagnetic coupling and/or zero-field splitting along the $\{Co(OCO)\}_n$ *anti–syn* bridged chain motifs. The $\chi_m T$ value for **2** at 300 K is $2.64\,cm^3\,K\,mol^{-1}$, which diminishes slowly to $2.50\,cm^3\,K\,mol^{-1}$ at 100 K, and reaches a minimum of $1.91\,cm^3\,K\,mol^{-1}$ at 12 K. Below this temperature the $\chi_m T$ value increases again, reaching $2.32\,cm^3\,K\,mol^{-1}$ at 2 K. Inspection of this curve portends the predomination of single-ion effects at higher temperature, with ferromagnetic coupling between adjacent cobalt ions making its presence felt at lower temperature. Modeling of the data over the entire temperature range with the Rueff expression (Eq. (2)) gives $D=38.4(4)\,cm^{-1}$, $J=0.324(5)\,cm^{-1}$, and $C=2.942(5)\,cm^3\,K\,mol^{-1}$ (which gives $g=2.504(2)$), with $R=1.04\times10^{-4}$ (Fig. 14). The small positive value of $J$ indicates very weak ferromagnetic coupling along the $\{Co(OCO)\}_n$ *anti–syn* bridged chains, by means of magnetic $d$ orbital interaction through the delocalized molecular orbitals of the carboxylate bridges. A study of magnetization versus applied field at 2 K revealed no hysteresis.

The magnetic susceptibility data of compound **3**, which also contains $\{Co(OCO)\}_n$ *anti–syn* bridged chains, was dealt with in like manner. A Curie–Weiss plot of the data above 50 K (Fig. S6) gave $C=2.91\,cm^3\,K\,mol^{-1}$ and $\Theta=-29.7\,K$, a preliminary indication of possible antiferromagnetic coupling and/or zero-field splitting (Fig. S11). The $\chi_m T$ value for **3** at 300 K is $2.65\,cm^3\,K\,mol^{-1}$, which decreases to $2.23\,cm^3\,K\,mol^{-1}$ at 100 K, and reaches a minimum of $1.56\,cm^3\,K\,mol^{-1}$ at 6 K. Below this temperature the $\chi_m T$ value increases, reaching $1.82\,cm^3\,K\,mol^{-1}$ at 2 K. Modeling of the data over the entire temperature range with the Rueff expression (Eq. (2)) gives $D=48.0(9)\,cm^{-1}$, $J=0.24(1)\,cm^{-1}$, and $C=2.93(1)\,cm^3\,K\,mol^{-1}$ (which gives $g=2.50(2)$), with $R=4.1\times10^{-4}$ (Fig. 15). It is thus plausible that both zero-field splitting and ferromagnetic coupling along the $\{Co(OCO)\}_n$ chains are operating in tandem.

Compound **4**, like **1**, contains $\{Co_2(OCO)_2\}$ dimers, so its variable temperature magnetic susceptibility data were analyzed similarly. A Curie–Weiss plot of the data above 30 K (Fig. S12) afforded $C=2.54\,cm^3\,K\,mol^{-1}$ and $\Theta=-20.9\,K$, indicating plausible antiferromagnetic coupling and zero-field splitting. The presence of these phenomena is corroborated by the variable temperature $\chi_m T$ data, which shows decreasing values ($2.39\,cm^3\,K\,mol^{-1}$ at 300 K, $2.04\,cm^3\,K\,mol^{-1}$ at 100 K, and $0.84\,cm^3\,K\,mol^{-1}$ at 2 K. An attempted fit of the data to the dimeric $S=3/2$ isotropic model (Eq. (1)) failed, with a very poor $R$ value of 0.16. Applying the Rueff expression to this dimeric case was once again

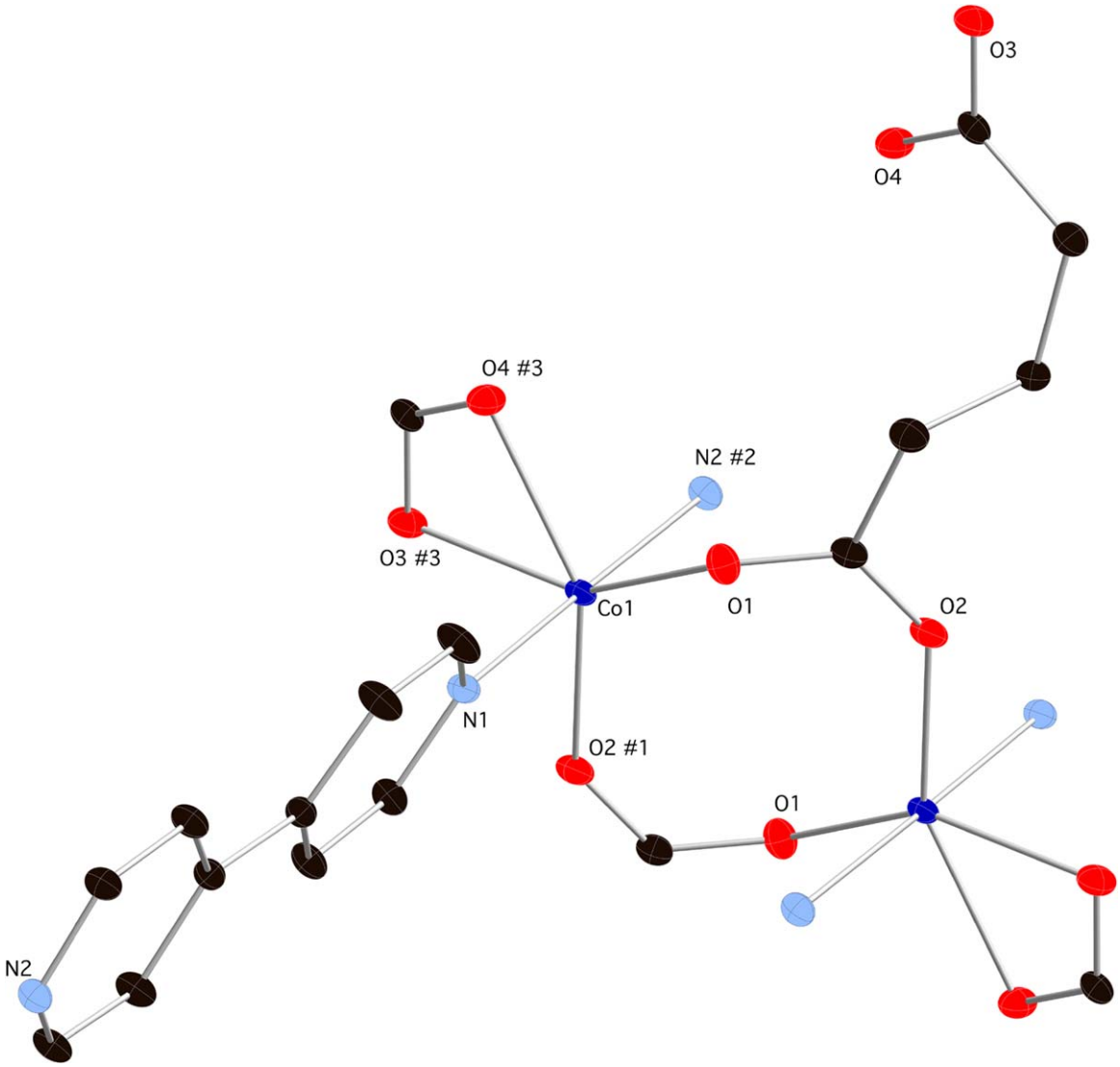


**Fig. 11.** Coordination environment of **5** with thermal ellipsoids shown at 50% probability. A complete $\{Co(OCO)\}_2$ dimeric unit is shown. The symmetry codes refer to those listed in Table 6.

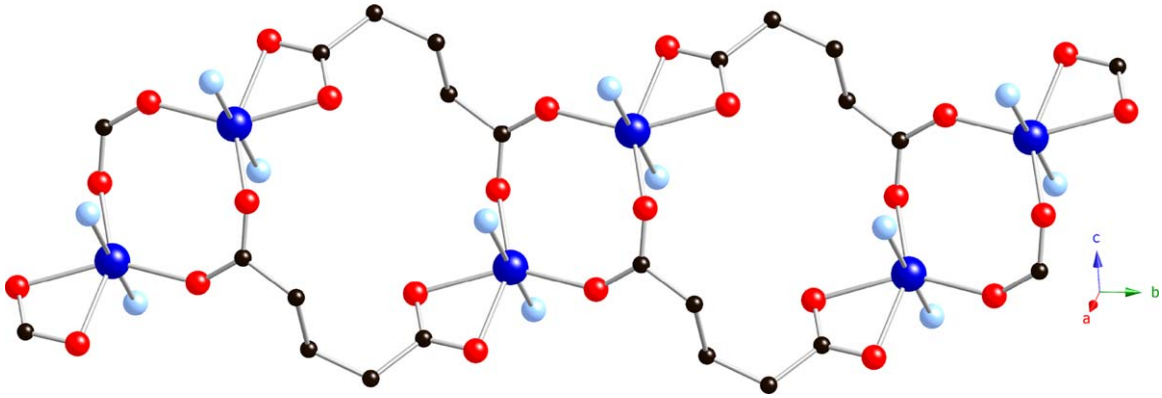


**Fig. 12.** A single $[Co(glu)]_n$ chain in **5**. The glutarate ligands adopt a *gauche–anti* conformation.

extremely successful. The best fit to Eq. (2) over the entire temperature range for **4** resulted in $D=37.6(5)\,cm^{-1}$, $J=-0.89(2)\,cm^{-1}$, and $C=2.594(6)\,cm^3\,K\,mol^{-1}$ (which gives $g=2.35(3)$), with $R=1.91\times10^{-4}$ (Fig. 16). The weaker antiferromagnetic coupling across the $\{Co_2(OCO)_2\}$ dimers in **4** can be plausibly ascribed to the longer Co···Co distance across the dimeric units (4.243 Å in **4**, 4.004 Å in **1**). The larger $D$ value in **4** is possibly correlated to greater deviations from idealized octahedral coordination geometry than in **1**. A summary of the relevant magnetic data for **1**–**4** is given in Table 7.

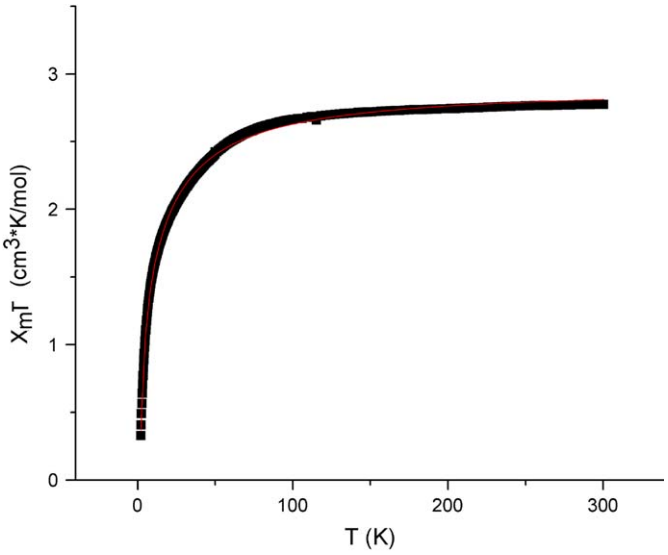


**Fig. 13.** Variable temperature $\chi_m T$ plot for **1**. The best fit to Eq. (2) is shown as a thin line.

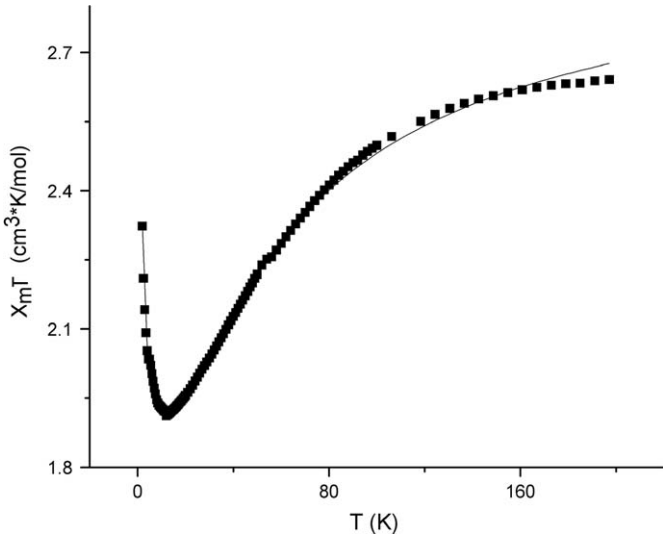


**Fig. 14.** Variable temperature $\chi_m T$ plot for **2**. The best fit to Eq. (2) is shown as a thin line.

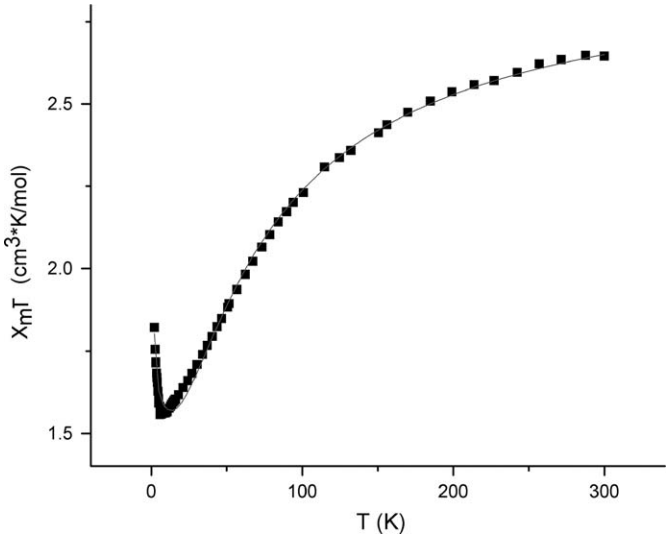


**Fig. 15.** Variable temperature $\chi_m T$ plot for **3**. The best fit to Eq. (2) is shown as a thin line.

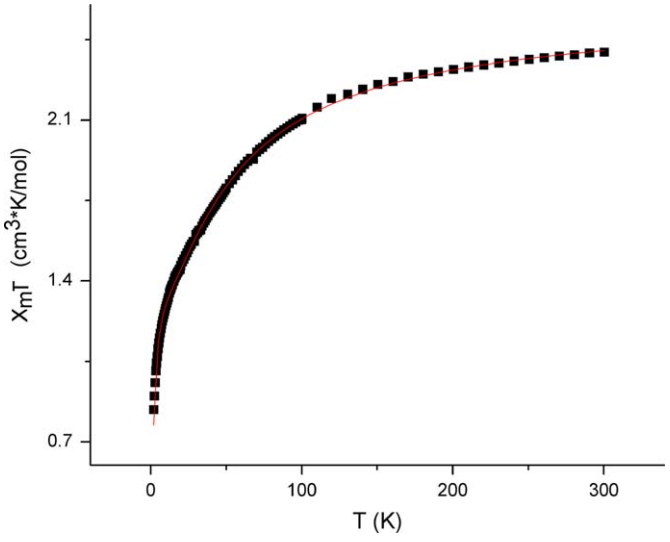


**Fig. 16.** Variable temperature $\chi_m T$ plot for **4**. The best fit to Eq. (2) is shown as a thin line.

### 4.8. Thermogravimetric analysis

Polycrystalline samples of **1** and **2** were subjected to thermogravimetric analysis to investigate the thermal stability of representative $\{Co_2(OCO)_2\}$ dimer-containing and $\{Co(OCO)\}_n$ chain-containing coordination polymers, respectively. Compound **1** underwent virtually no mass loss between 25 and 290 °C, whereupon expulsion of the organic components occurred. All ligands were ejected by ~420 °C. The 22.5% mass remnant at 500 °C roughly corresponds to a deposition of CoO (20.9% predicted). Dehydration of compound **2** occurred in two steps, one completed at ~100 °C, the second at ~120 °C. The mass loss of 10.8% is consistent with the expulsion of all ligated and co-crystallized water molecules (12.0% predicted). Mass loss was minimal between ~120 and ~200 °C, with an accelerating decrease in mass thereafter. The 20.0% remnant at 600 °C matches acceptably with a deposition of CoO (17.5% predicted). Thermograms for **1** and **2** are shown in Figs. S13 and S14, respectively.

**Table 7**
Magnetic data for **1**–**4**.

| Compound | $g$ | J ($cm^{-1}$) | $D$ ($cm^{-1}$) |
|---|---|---|---|
| **1** | 2.49(2) | −2.43(4) | 21.8(8) |
| **2** | 2.504(2) | +0.324(5) | 38.4(4) |
| **3** | 2.50(2) | +0.24(1) | 48.0(9) |
| **4** | 2.35(3) | −0.89(2) | 37.6(5) |

## 5. Conclusion

Altering the substituents at the 3-position of glutarate ligands has shown a significant effect on the resulting topology in a divalent cobalt/4,4′-bipyridine coordination polymer system. A small degree of steric bulk in 3-methylglutarate did not appreciably change the coordination polymer topology from the dimer-containing (4,4) rhomboid grid seen in a related unsubstituted glutarate phase. The presence of two alkyl group

substituents (in either 3,3-dimethylglutarate or 3-ethyl, 3-methylglutarate) resulted in a wholesale alteration of the topology, producing "infinite" 1-D $\{Co(OCO)\}_n$ chains linked into 2-D by bpy ligands. Nevertheless, "tying back" the two alkyl susbstituents by means of a cyclopentane ring caused a reversion to the original dimer-based grid coordination polymer topology. As expected, the sterically unhindered, unsubstituted glutarate ligand gave a dimer-based structure, however a conformational change in the aliphatic chain from *gauche–gauche* to *gauche–anti* resulted in a wider spacing between dimer units and therefore an alteration of lattice parameters.

Variation of coordination polymer topology caused significant changes in magnetic properties. While the variable temperature magnetic susceptibility data for all four complexes show a significant zero-field splitting effect, the dimer-containing compounds **1** and **4** exhibit antiferromagnetic coupling, while the chain-based complexes **2** and **3** show ferromagnetic coupling between adjacent cobalt ions. Within **1** and **4**, each pair of adjacent cobalt ions is bridged by a pair of carboxylate groups in a *syn–syn* orientation. On the other hand, within **2** and **3**, each pair of adjacent cobalt ions is bridged by only a single carboxylate group, in a *syn–anti* orientation. It is likely that the specific magnetic orbital interactions provided by these structural factors results in the different magnetic behavior between the antiferromagnetic **1** and **4**, and ferromagnetic **2** and **3**. This work also shows the applicability of Rueff's phenomenological model for chains of $S=3/2$ spins to dimeric systems that do not follow isotropic Heisenberg behavior because of anisotropy, thus allowing estimates of the comparative effects of zero-field splitting and magnetic superexchange.

## Supplementary material

Crystallographic data for **1–5** have been deposited with the Cambridge Crystallographic Data Centre with the deposition numbers 735729, 735730, 735731, 735732, and 737608, respectively. Copies of the data can be obtained free of charge via the Internet at http://www.ccdc.cam.ac.uk/conts/retrieving.html or by post at CCDC, 12 Union Road, Cambridge CB2 1EZ, UK; fax: (+44) 1223-336-033; or email: deposit@ccdc.cam.ac.uk. Additional molecular graphics, Curie–Weiss plots and thermograms can be obtained through the online version of this article.

## Acknowledgments

The authors gratefully acknowledge the donors of the American Chemical Society Petroleum Research Fund for financial support of this work. We thank Dr. Rui Huang for elemental analysis and Dr. Reza Loloee for instruction in the use of the SQUID magnetometer.

## Appendix A. Supplementary material

Supplementary data associated with this article can be found in the online version at doi:10.1016/j.jssc.2009.11.015.

## References

[1] [a] J.L.C. Roswell, O.M. Yaghi, Angew. Chem. Int. Ed. Engl. 44 (2005) 4670;
[b] M. Kondo, T. Okubo, A. Asami, S.I. Noro, T. Yoshitomi, S. Kitagawa, T. Ishii, H. Matsuzaka, Angew. Chem. Int. Ed. Engl. 38 (1999) 140;
[c] A.C. Sudik, A.R. Millward, N.W. Ockwig, A.P. Cote, J. Kim, O.M. Yaghi, J. Amer. Chem. Soc. 127 (2005) 7110;
[d] A.K. Cheetham, C.N.R. Rao, R.K. Feller, Chem. Commun. (2006) 4780.
[2] [a] J.S. Seo, D. Whang, H. Lee, S.I. Jun, J. Oh, Y.J. Jeon, K. Kim, Nature 404 (2000) 982;
[b] A. Cingolani, S. Galli, N. Masciocchi, L. Pandolfo, C. Pettinari, A. Sironi, J. Amer. Chem. Soc. 127 (2005) 6144.
[3] [a] Q.R. Fang, G.S. Zhu, M. Xue, J.Y. Sun, S.L. Qiu, Dalton Trans. (2006) 2399;
[b] X.M. Zhang, M.L. Tong, H.K. Lee, X.M. Chen, J. Solid State Chem. 180 (2001) 118;
[c] O.M. Yaghi, H. Li, T.L. Groy, Inorg. Chem. 36 (1997) 4292.
[4] [a] S.G. Baca, M.T. Reetz, R. Goddard, I.G. Filippova, Y.A. Simonov, M. Gdaniec, N. Gerbeleu, Polyhedron 25 (2006) 1215;
[b] H. Han, S. Zhang, H. Hou, Y. Fan, Y. Zhu, Eur. J. Inorg. Chem. (2006) 1594;
[c] W. Mori, S. Takamizawa, C.N. Kato, T. Ohmura, T. Sato, Microporous and Mesoporous Materials 73 (2004) 15;
[d] F. Gandara, B. Gomez-Lor, M. Iglesias, N. Snejko, E. Gutierrez-Puebla, A. Monge, Chem. Commun. (2009) 2393;
[e] M. Wang, M.H. Xie, C.D. Wu, Y.G. Wang, Chem. Commun. (2009) 2396.
[5] [a] S. Zang, Y. Su, Y. Li, Z. Ni, Q. Meng, Inorg. Chem. 45 (2006) 174;
[b] L. Wang, M. Yang, G. Li, Z. Shi, S. Feng, Inorg. Chem. 45 (2006) 2474;
[c] S. Wang, Y. Hou, E. Wang, Y. Li, L. Xu, J. Peng, S. Liu, C. Hu, New J. Chem. 27 (2003) 1144;
[d] Y.F. Zhou, D.Q. Yuan, B.L. Wu, R.H. Wang, M.C. Hong, New J. Chem. 28 (2004) 1590;
[e] G.W. Zhou, Y.Z. Lan, F.K. Zheng, X. Zhang, M.H. Lin, G.C. Guo, J.S. Huang, Chem. Phys. Lett. 426 (2006) 341;
[f] L. Han, M. Hong, R. Wang, J. Luo, Z. Lin, D. Yuan, Chem. Commun. (2003) 2580.
[6] W.G. Lu, C.Y. Su, T.B. Lu, L. Jiang, J.M. Chen, J. Amer. Chem. Soc. 128 (2006) 34.
[7] S. Horike, R. Matsuda, S. Kitagawa, Studies in Surface Sci. Cat. 156 (2005) 725.
[8] C. Qin, X.L. Wang, Y.G. Li, E.B. Wang, Z.M. Su, L. Xu, R. Clerac, Dalton Trans. (2005) 2609.
[9] Y.Q. Zheng, E.R. Ying, Polyhedron 24 (2005) 397.
[10] S.K. Ghosh, J. Ribas, P.K. Bharadwaj, Crystal Growth Des. 5 (2005) 623.
[11] X.Z. Sun, Y.F. Sun, B.H. Ye, X.M. Chen, Inorg. Chem. Commun. 6 (2003) 1412.
[12] L. Xu, G.C. Guo, B. Liu, M.S. Wang, J.S. Huang, Inorg. Chem. Commun. 7 (2004) 1145.
[13] H.P. Jia, W. Li, Z.F. Ju, J. Zhang, Eur. J. Inorg. Chem. (2006) 4264.
[14] B. Chen, C. Liang, J. Yang, D.S. Contreras, Y.L. Clancy, E.B. Lobkovsky, O.M. Yaghi, S. Dai, Angew. Chem. Int. Ed. 45 (2006) 1390.
[15] M. Kurmoo, Chem. Soc. Rev. 38 (2009) 1353.
[16] S. Xiang, X. Wu, J. Zhang, R. Fu, S. Hu, X. Zhang, J. Amer. Chem. Soc. 127 (2005) 16352.
[17] X.-Y. Wang, S.C. Sevov, Inorg. Chem. 47 (2008) 1037.
[18] Y.-G. Huang, D.-Q. Yuan, L. Pan, F.-L. Jiang, M.-Y. Wu, X.-D. Zhang, W. Wei, Q. Gao, J.Y. Lee, J. Li, M.-C. Hong, Inorg. Chem. 46 (2007) 9609.
[19] [a] Y. Hu, G. Li, X. Liu, B. Hu, M. Bi, L. Gao, Z. Shi, S. Feng, Cryst. Eng. Comm. 10 (2008) 888;
[b] M.-H. Zeng, W.-X. Zhang, X.-Z. Sun, X.-M. Chen, Angew. Chem. Int. Ed. 44 (2005) 3079.
[20] [a] L.-S. Long, Y.-R. Wu, R.-B. Huang, L.-S. Zheng, Inorg. Chem. 43 (2004) 3798;
[b] P.S. Mukherjee, S. Konar, E. Zangrando, T. Mallah, J. Ribas, N.R. Chaudhuri, Inorg. Chem. 42 (2003) 2695;
[c] L. Pan, H. Liu, X. Lei, X. Huang, D.H. Olson, N.J. Turro, J. Li, Angew. Chem. Int. Ed. 42 (2003) 542;
[d] F.S. Delgado, M. Hernandez-Molina, J. Sanchiz, C. Ruiz-Perez, Y. Rodriguez-Martin, J. Lopez, F. Lloret, M. Julve, Cryst. Eng. Comm. 6 (2004) 106.
[21] B. Rather, M.J. Zaworotko, Chem. Commun. (2003) 830.
[22] B. Chen, Y. Li, M. Xue, F.R. Fronczek, E.J. Hurtado, J.U. Mondal, C. Liang, S. Dai, Inorg. Chem. 47 (2008) 5543.
[23] J.H. Nettleman, P.J. Szymanski, L.K. Sposato, R.L. LaDuca, Inorg. Chim. Acta. 363 (2010) 225.
[24] O. Khan, Molecular Magnetism, VCH Publishers, New York, 1993.
[25] SAINT, Software for Data Extraction and Reduction, Version 6.02, Bruker AXS Inc., Madison, WI, 2002.
[26] SADABS, Software for Empirical Absorption Correction, Version 2.03, Bruker AXS Inc., Madison, WI, 2002.
[27] G.M. Sheldrick, SHELXTL Program for Crystal Structure Refinement, University of Gottingen, Gottingen, Germany, 1997.
[28] M. Kurmoo, C. Estournes, Y. Oka, H. Kumagai, K. Inoue, Inorg. Chem. 44 (2005) 217.
[29] Y.-Q. Zheng, J.-L. Lin, Z.-P. Kong, Inorg. Chem. 43 (2004) 2590.
[30] A.L. Spek, PLATON, A Multipurpose Crystallographic Tool, Utrecht University, Utrecht, The Netherlands, 1998.
[31] J.M. Rueff, N. Masciocchi, P. Rabu, A. Sironi, A. Skoulios, Eur. J. Inorg. Chem. (2001) 2843.